Errors Impacts of Multi-5G Waveforms in Cognitive Radio Systems

Mokhalad Alghrairi, Aqeel k. Kadhim, Manar Adnan Nassrat, Bayan Mahdi Sabbar, and Saad Mutashar

***Abstract*—The demand for new wireless services within frequency bands has increased due to the exponential growth of wireless communication, leading to issues related to spectrum scarcity. This paper proposes a hybrid technique-based Spectrum Sensing (SS) algorithm. The traffic signal filtering component of the method utilizes the cosine law in conjunction with the Welch algorithm for segmentation. It incorporates various 5G waveforms, including Generalized Frequency Division Multiplexing (GFDM), Filtered Orthogonal Frequency Division Multiplexing (F-OFDM), Filter Bank Multi-Carrier (FBMC), Non-Orthogonal Multiple Access (NOMA), and Universal Filtered Multi-Carrier (UFMC). The (SS) system achieves a false alarm rate of less than 0.05, a detection probability (Pd) greater than 0.95, and a system error probability of less than 0.09%. Key metrics are used to evaluate the algorithm's performance, and simulation results demonstrate its capability to distinguish between different types of 5G signals.**

***Index terms*—cognitive radio, 5G, probability of detection, probability of false alarm, error probability.**

I. Introduction

The growing demand for increased data capacity in the evolving realm of communication, driven by the significant surge in annual data traffic, has become a major challenge [1, 2]. The imminent introduction of fifth-generation (5G) technology, with its multi-gigabit-per-second capability, is seen as a promising solution to address this escalating need [3, 4].

Beyond catering to the need for faster data speeds, 5G is anticipated to revolutionize various cutting-edge technologies, such as virtual reality, smart cities, and the Internet of Vehicles.

Nevertheless, there are hurdles hindering the implementation of 5G technology, particularly the scarcity of spectrum, which is aggravated by the rigid allocation of radio resources [5, 6]. A potential remedy for this dilemma is the suggestion of cognitive radio (CR) technology for dynamic spectrum access (DSA). Secondary users (SUs) can utilize cognitive radio to access licensed spectrum that primary users (PUs) are not currently using, while closely monitoring PU activities to prevent interference [7, 8]. Furthermore, to ensure effective spectrum utilization and reliable connectivity, 5G communication networks must work harmoniously with multi-input, multi-output (MIMO) technology. MIMO systems, which involve multiple antennas, pose challenges due to increased complexity, even though they offer advantages, particularly in detecting signals under low signal-to-noise ratio (SNR) conditions [9].

The latest investigation suggests a hybrid technique (HT) strategy for detecting 5G MIMO signals to address the issue of spectrum scarcity [10]. This study is driven by the increasing demand for services and the strain it places on spectrum capacities. The primary concern highlighted is the availability of spectrum, which makes it difficult to offer wireless services and necessitates the use of complex (SS) algorithms [11]. In this paper, the error ratio of multiple 5G waveforms is investigated and analyzed. These waveforms include Universal Filtered Multi-Carrier (UFMC), Filtered Orthogonal Frequency Division Multiplexing (F-OFDM), Filter Bank Multi-Carrier (FBMC), Non-Orthogonal Multiple Access (NOMA), and Generalized Frequency Division Multiplexing (GFDM). The proposed model is based on the SNR wall, probability of false alarm, and probability of detection. This model analyzes several (SS) techniques, such as the hybrid technique, log-likelihood ratio technique, and energy detection technique. It represents a flexible and promising solution to the challenges presented by the evolving wireless communication landscape.

The paper is divided into several sections: the literature review, the reasons, and the main contributions outlined in Sections II and III. In Section IV, the mathematical framework of the recommended hybrid technique is evaluated, and the system structure and formulation are further elaborated upon. The outcomes of the simulation are presented in Section V, where the error probability observations between the proposed (SS) strategy and conventional techniques are compared. Section VI concludes by summarizing the findings and outlining potential avenues for further investigation.

II. Literature Review

Various approaches have been proposed for analyzing 5G networks, each with its own set of benefits and drawbacks. The K-best technique, which showed promise in machine learning applications in 2015, struggled to minimize errors across all 5G competitors when applied to MIMO-FBMC networks that depend on coded and iterative decoding (IDs) [7]. A later attempt to implement factor graph (FG)-based soft-input-soft-output (SISO) (maximum-a-posterior) MAP detection for

Manuscript received October 14, 2024; revised December 9, 2024. Date of publication March 25, 2025. Date of current version March 25, 2025. The associate editor prof. Giovanni Giambene has been coordinating the review of this manuscript and approved it for publication.

M. Alghrairi and A. k. Kadhim are with the Department of Computer Techniques Engineering, Imam Alkadhim University College, Baghdad, Iraq (e-mails: mokhalad.khaleel@iku.edu.iq, compeng.lecturer4@alkadhum-col.edu.iq).

M. A. Nassrat is with the Optics Technique Department, Al-Hikma University College, Baghdad, Iraq (e-mail: manar.adnan@hiuc.edu.iq).

B. M. Sabbar and S. Mutashar are with the Medical Instrumentation Techniques Engineering Department, Al-Mustaqbal University, Hillah, Iraq (e-mails: {prof.dr.bayan.mahdi, Saad.Mutashar.abbas}@uomus.edu.iq).

Digital Object Identifier (DOI): 10.24138/jcomss-2024-0050

FBMC systems in 2015 encountered significant complexity challenges [12].

In 2017, researchers investigated inter-subband-interference (ISubBI) cancellation techniques to develop a multi-rate F-OFDM approach aimed at lowering both initial OFDM complexity and error rates in low-cost networks [13]. While they worked on conditional techniques such as Partial Transmit Sequences (PTS) and hybrid processing strategies in 2019 to reduce Peak-to-Average Power Ratio (PAPR) in FBMC- offset quadrate amplitude modulation (OQAM) networks [14], those efforts partially succeeded but did not resolve critical issues related to complexity and error levels. During the same year, MIMO C-FBMC information detection displayed improved capability, though it still failed to mitigate error probabilities for all 5G contenders [15].

Although it presented greater complexity, a comparative study of FBMC-OQAM, Polyphase Network (PPN)-FBMC, and FS-FBMC receiver architectures in a single year favored FS-FBMC [16]. Even though the unique HDFT-based FS-FBMC design achieved a reduction in complexity from high to moderate levels, challenges in error management persisted. A proposal to lower the computational demands of F-OFDM emerged in 2019 [17]; however, even with the removal of restrictions on the F-OFDM filter length, significant computational complexity continued to exist, making it unsuitable for all 5G scenarios. Additionally, a technique based on pairwise error likelihood for RB-F-OFDM networks was introduced the same year to alleviate error rates, but it could not effectively manage elevated complexity [18].

In 2020, a study comparing FBMC wireless networks with fewer subcarriers highlighted their superior inherent efficiency compared to OFDM networks, despite a higher probability of errors [19]. These error levels remained problematic. A 2020 evaluation of inaccuracies and complexities in UFMC-based methods underscored the merits of lightweight systems that combined polyphase and FIR filters [20]. However, the methods explored struggled to adequately address the associated error probabilities, despite efforts to propose solutions. Additionally, that year, a Selected Mapping (SLM) approach demonstrated potential by streamlining the operation of UFMC modulators [21].

After a thorough evaluation of these existing methods, the authors concluded that current techniques failed to adequately tackle the growing likelihood of errors. In light of this, a novel technique based on Cognitive Radio Networking (CRN) is proposed within a Hybrid Technique (HT) framework to differentiate among 5G waveforms, with a particular focus on SNR values and reduced inaccuracies. This HT combines factors such as system error and false alarm probabilities, SNR thresholds, and detection rates without requiring primary user knowledge. To differentiate between traffic and noise, cosine filters are utilized within the framework for assessing white bands. The Welch technique is subsequently applied for the segmentation of target signals.

III. Motivation and Main Contributions

This work is motivated by the ongoing shortage of spectrum resources in wireless systems, particularly concerning 5G terrestrial systems that lack cognitive radio networks capable of recognizing different types of waveforms. Issues such as a high error rate and poor signal detection performance in low signal-to-noise ratio (SNR) environments further contribute to the overall decline in performance quality and efficiency. The proposed Cognitive Radio 5G (CR-5G) technologies employ high-data-rate transmission and reception to overcome these challenges and improve both non-cooperative (SS) and the various requirements of 5G waveforms.

The investigation utilizes a multifaceted approach that incorporates (HT) in cognitive radio and (MIMO) systems to address these difficulties. The principal contributions of this method are as follows:

A) Providing a method for accurately detecting 5G waveforms: The blind (SS) technique comprises two consecutive steps: Welch-based segmentation and cosine filtering to differentiate 5G traffic from noise. In this process, Welch segmentation filtering precedes the segmentation of the desired signal, effectively reducing the residual noise variance. The Power Spectral Density (PSD) of each segment is calculated, and the presence of the signal is determined by comparing the average PSD values (test statistic) with a predetermined threshold. This methodology ensures rapid detection, addresses low SNR issues, distinguishes signal variance from noise, and minimizes errors.

B) Using MIMO uncooperative and cooperative (SS) techniques to identify multiple waveforms: This approach detects various waveform types, such as F-OFDM, GFDM, UFMC, NOMA, and FBMC, rather than focusing on a single waveform type, thus increasing throughput and spectral efficiency.

C) Demonstrating that the proposed (SS) technology detects signals more accurately and with a reduced likelihood of error.

IV. Formulation and Model of the System

It is believed that using a binary hypothesis is an effective method for establishing the sensing procedure. This method involves two hypotheses: the null hypothesis (H_0) and the alternative hypothesis (H_1). The null hypothesis (H_0) represents the case when the communication band is inactive, meaning that the received signal consists solely of background noise. In contrast, the alternative hypothesis (H_1) indicates that the band is occupied, signifying that both traffic and noise are present in the received signal. This binary hypothesis framework is followed by the notations and representations used in the present article.

In summary, the busy scenario implies that both noise and traffic exist in the band, while the idle scenario indicates that only noise is present within the band [22]. As a result, each hypothesis is deduced based on the error rate, as demonstrated here.

A. Background formulation

In short, the busy scenario refers to a situation where both noise and traffic are present in the band, while the idle scenario implies that only noise is found within the band [22]. Consequently, each hypothesis is derived from the rate of errors, as illustrated below:

$$P_f = P(\text{Decision} = H_1|H_0) \quad (1)$$

$$P_{md} = P(Decision = H_0|H_1) \quad (2)$$

hence,

$$P_e = P_f + P_{md} \quad (3)$$

The probability of a false alarm (Type I error) is represented by Pf which indicates an inaccurate detection of a primary user (PU) signal. Additionally, P_{md} represents the likelihood of a missed detection (Type II error), which reflects precise sensing concerning PU signals. P_e denotes the overall system fault probability. The (Pd) is defined as the complement of the missed detection probability, as expressed below:

$$P_d = P(Decision = H_1|H_1) \quad (4)$$

hereafter,

$$P_{md} + P_d = 1 \quad (5)$$

The simple energy detection method can be used to build a blind sensor waveform. It provides all information pertaining to the construction of signals. By matching the received power and a particular threshold γ calculated via noise computations, it employs sign approximation. There are two potential options for the (SS) technique:

$$H_0: PU\ Absen \ldots S[n] = w[n] \quad (6)$$

$$H_1: PU\ Present \ldots S[n] = s[n] + w[n] \quad (7)$$

while w[n] represents noise samples, which are regarded as additive white Gaussian noise (AWGN), s[n] represents the most important signals, and M indicates the duration of the detection procedure, Meanwhile S[n] contains samples that resemble the received waveform.

B. Problem formulation

The eighth equation is used to determine the signal energy level, after which test statistic G is identified by comparing to the given value as:

$$G = 1/M \sum_{n-1}^{M} S(n)^2 \quad (8)$$

where K denotes energy detector output, N denotes the bin count, while S[n] denotes the complex digitized waveform. In (9), for every hypothesis, where σ_w^2 denotes noise process variance and σ_s^2:

$$G - M(M\sigma_w^2, 2M\sigma_w^4)\ under\ H_0 \quad (9)$$

The suggested strategy assumes that the length of the PU signal is N in order to rewrite the binary hypothesis using the characteristics of the transmitted signal. It is assumed that G is the sum of squares for N Gaussian random variables. According to the central limit theorem [8], the distribution of G thus approximates a normal distribution when N > 250. The following explains how the mean and variance are formulated:

$$G - M(N(\sigma_w^2 + \sigma_s^2), 2N(\sigma_w^2 + \sigma_s^2)^2)\ \ under\ H_1 \quad (10)$$

Starting now the primary aim of λD, for the user signal is as follows: PFA and (Pd) are analyzed statistically, with G representing the test statistic that needs to be compared to a predefined threshold defined by:

$$P_{FA} = P_r(G > \lambda_D: H_0) \quad (11)$$

$$P_D = P_r(G > \lambda_D: H_1) \quad (12)$$

The values of the factors for the (Pd) and the likelihood of false alarm (Pf) are commonly utilized for evaluating the efficacy of (SS) in relation to non-cooperative users, as defined in Equations (13) and (14), wherein G represents the test statistic established in (9). The probability that the SU will falsely claim to be transmitting as a licensed user (PU) while, in reality, there are none on the spectrum is known as Pf. [23]:

$$P_f = Prob\{(H_1 \backslash H_0)\} = Q\left(\frac{\boldsymbol{\lambda D} - \sigma_w^2}{\sqrt{\frac{2}{M}}\sigma_w^2}\right) \quad (13)$$

$$P_d = Prob\{(H_0 \backslash H_1)\} = Q\left(\frac{\boldsymbol{\lambda D} - (\sigma_w^2 + \sigma_s^2)}{\sqrt{\frac{2}{M}}(\sigma_w^2 + \sigma_s^2)}\right) \quad (14)$$

where Q stands for the tail likelihood related to the standard typical distribution. Formula (13) can be used to indicate the application of the (SS) method for the false alarm likelihood in the recommended MIMO systems (GFDM, FBMC, UFMC, F-OFDM, and NOMA) in accordance with energy detection:

$$P_f = Prob\{(H_1 \backslash H_0)\} = Q\left(\frac{G - R(2\,\sigma_w^2}{\sqrt{\frac{2R}{M}}(\sigma_w^2)2}\right) \quad (15)$$

An increase in the false alarm likelihood indicates that the SU has taken advantage of the window for spectrum utilization during periods when the PU is not operational. To maximize spectrum efficiency, it is imperative that the false alarm probability be minimized to the lowest achievable level [24]. The fifteenth equation provides information about the factors that affect the likelihood of a false alarm, including the threshold, the number of receiver antennas, the number of samples used in the detection process, and the noise variance. On the other hand, detection likelihood describes the probability that, whenever the PU truly exists, the SU will correctly declare the existence of a licensed user and begin to utilize the spectrum for transmission [25]. Equation fourteen (14) describes how the squaring technique implements (SS) through energy detection for the suggested MIMO systems (GFDM, FBMC, UFMC, F-OFDM, and NOMA) of communication:

$$P_d = Prob\{(H_0 \backslash H_1)\} = Q\left(\frac{\mathbf{G - 2R} - (\sigma_w^2 + \sigma_s^2)}{\sqrt{\frac{2R}{M}}(\sigma_w^2 + \sigma_s^2)2}\right) \quad (16)$$

The proposed work is assessed using the Receiver Operating Characteristic (ROC) curve related to the (SS) technique in order to ascertain the detector's efficiency. The relationship between Pf and (Pd) indicates that optimal detection

performance is achieved when Pf remains lower and (Pd) is higher, which is related to the ROC. The primary user (PU) will be protected while the secondary user (SU) can utilize the spectrum more efficiently if Pf is lower and (Pd) is greater. Using (10), the threshold is derived as follows:

$$\lambda_D = \sigma_w^2\left(Q^{-1}(P_{FA})\sqrt{2M} + M\right) \quad (17)$$

The sensing decision is performed as:

$$if\ \lambda_D \geq G \qquad H_1 \quad (18)$$

$$if\ \lambda_D \geq G \qquad H_0 \quad (19)$$

while PSDt indicates the total PSD as well as λ stands for the predetermined threshold.

C. 5G Waveforms formulation

One component of the sub-band MCM technique is F-OFDM, which includes a flexible filtering mechanism. As such, it can be practically used for various characteristics, including bandwidth, transmission time interval, and Cyclic Prefix (CP) period. Acceptable complexity and sufficient immunity are two benefits of using F-OFDM over transmission non-coherence. It can also be applied in conjunction with the MIMO methodology [26, 27]. Before defining the mathematical foundation of the F-OFDM method, the basic formulation of the baseband signal in OFDM is presented:

$$x_{F-OFDM}(v) = \sum_{b=0}^{B-1}\sum_{m=0}^{M-1}\sum_{l=0}^{L-1}\sum_{n=0}^{N-1} s_{m,n}^{b} g_b[l] e^{j2\pi v\frac{(n-l-mC_P)}{N}} \quad (20)$$

Whereas the Cyclic Prefix (CP) provides the CP size, gb[1] points to the frequency corresponding to the prototype filter that has a finite impulse response for the b-th block of length l. Furthermore, the information sent for the b-th block, n-th subcarrier, and m-th sub-symbol is indicated by sbm, n [28, 29]. On the other hand, UFMC is regarded as a viable sub-band MCM technique with a unique filtering scheme. Given that the technique divides bandwidth into specific subdivisions that correspond to the frequency domain, it is less flexible than F-OFDM in terms of efficiency. Since the CP element is not considered in any conventional UFMC technique, receiving signals transmitted by UFMC requires a highly developed receiver. To address this, the UFMC receiver utilizes an FFT that is twice as large as the IFFT used by the UFMC transmitter. In conclusion, the UFMC technique has the potential to reduce time-frequency offsets, making it ideal for addressing low latency issues [30, 31]. The baseband signals of the UFMC method are defined using the following definitions:

$$x_{UFMC}(v) = \sum_{b=0}^{B-1}\sum_{l=0}^{L-1}\sum_{n=0}^{N-1} s_n^b g[l] e^{j2\pi v\frac{(n-l)}{N}} \quad (21)$$

The frequencies set at the finite impulse response filters are represented by g[l] and sbn, which convey the information that is sent. Furthermore, FBMC is regarded as a sub-carrier MCM technique that features a pulse shaping period that increases with respect to the time-domain filter. Three different filtering techniques have been employed: filtered multi-tone, staggered modulated multi-tone, and cosine modulated multi-tone. Since the transmitted symbols consist of both the real and imaginary parts of the delay, the filters used are orthogonal. Compared to UFMC, longer filters are utilized in the FBMC scenario. Additionally, the FBMC method outperforms OFDM in terms of spectrum utilization, attributable to the time- and frequency-domain safeguards [11, 32]. The following demonstrates how the FBMC method is represented:

$$x_{FBMC}(v) = \sum_{m=-\infty}^{\infty}\sum_{n=0}^{N-1} s_{m,n} g[k - m\tfrac{N}{2}] e^{j2\pi v\frac{n}{N}} e^{j\varphi_{m,n}} \quad (22)$$

An additional expression, denoted by φm,n, is given as (m+n)π/2. If the two symbol aspects—real and imaginary—are broadcast after a delay, the Sm,n value is taken into account. The following section discusses the (SS) approach used in this work for potential 5G waveforms, with a schematic shown in Figure 6. To develop the (SS) frequency domain approach for energy identification, we evaluated the modified cosine filter, as stated in the subsequent formulations. Processing the incoming signal with the cosine filter is the first stage [31]:

$$R[0] = \frac{\sqrt{2}}{V}\sum_{v=0}^{V-1} r[v], \quad k = 0 \quad (23)$$

$$R[k] = \frac{2}{V}\sum_{v=0}^{V-1} r[v]\cos\left(\frac{\pi k(2v+1)}{2V}\right), \quad 1 \leq k \leq K-1 \quad (24)$$

In which the obtained 5G signal, of length V, is denoted by r[v]. Following is a description of it:

$$\begin{cases} w[n] & H_0 \\ \mathbf{S[n]} = \begin{cases} NOMA\,[v] \\ F-OFDM\,[v] \\ FBMC[v] \\ GFDM[v] \\ UFMC[v] \end{cases} + w[n] & H_1 \end{cases} \qquad n = 1,2,\dots,n \quad (25)$$

wherein the Gaussian noise with zero mean and σ_w^2 variance is denoted by w[v]. Note that all 5G received signals were either xFBMC, xGFDM, xUFMC, xF-OFDM or xNOMA. These signals were assumed to be autonomous and had a variance of σ_s^2 and an identically distributed (i.i.d) random procedure. The matched filtered signal for S[n] is denoted by R[k].

D. Proposed Model Formulation

To cut down on the complexity of computation as well as sensing time, the null coefficients of R[k] must be removed in the second phase. R[k] is thus transformed to R' [k] and has a new length of K', where K' < K. Traffic can be carried out with the aid of a few samples. Using the Bartlett segmentation method, R' [k] was split into Nseg segments with Lseg length following the implementation of the cosine filter. Once that, every segment's PSD is determined after it has been windowed independently via the Hamming window. Last but not least, the final PSD (RPSD) was taken to be the average of the preceding

PSDs. The test statistic is derived from this mean RPSD. Each of the above stages has a mathematical description for the GFDM, FBMC, UFMC, F-OFDM, and NOMA candidates, in that order. Equation twenty-five depicts the modified F-OFDM signal using the cosine filter approach. Equation (33), on the other hand, shows the elimination of every one of its null coefficients:

$$R_{F-OFDM}[k] = (-1)^k \sum_{v=0}^{V-1}\sum_{b=0}^{B-1}\sum_{m=0}^{M-1}\sum_{l=0}^{L-1}\sum_{n=0}^{N-1} \frac{s_{m,n}^{b} g_b[l] e^{j2\pi v\frac{(n-l-mc)}{N}}}{\sqrt{V}} + \sqrt{\frac{2}{V}} \sum_{v=0}^{V-1}\sum_{b=0}^{B-1}\sum_{m=0}^{M-1}\sum_{l=0}^{L-1}\sum_{n=0}^{N-1} s_{m,n}^{b} g_b[l] e^{j2\pi v\frac{(n-l-mC)}{N}} \cos\left(\frac{\pi k(2v+1)}{2V}\right), \quad 0 \le k \le K-1 \qquad (26)$$

The equations (27) as well as (34) similarly show the modified UFMC signal as well as the removal of its null parameters, respectively:

$$R_{UFMC}[k] = (-1)^k \sum_{v=0}^{V-1}\sum_{b=0}^{B-1}\sum_{l=0}^{L-1}\sum_{n=0}^{N-1} s_n^b g[l] e^{j2\pi v\frac{(n-l)}{N}} \Big/ \sqrt{V} + \sqrt{\frac{2}{V}} \sum_{v=0}^{V-1}\sum_{b=0}^{B-1}\sum_{l=0}^{L-1}\sum_{n=0}^{N-1} s_n^b g[l] e^{j2\pi v\frac{(n-l)}{N}} \cos\left(\frac{\pi k(2v+1)}{2V}\right), \quad 0 \le k \le K-1 \qquad (27)$$

Equation (28) highlights the altered FBMC signal, while Equation (35) illustrates the removal of its null elements:

$$R_{FBMC}[k] = (-1)^k \sum_{v=0}^{V-1}\sum_{m=-\infty}^{\infty}\sum_{n=0}^{N-1} s_{m,n} g\left[k - m\frac{N}{2}\right] e^{j2\pi v\frac{n}{N}} e^{j\varphi_{m,n}} \Big/ \sqrt{V} + \sqrt{\frac{2}{V}} \sum_{v=0}^{V-1}\sum_{m=-\infty}^{\infty}\sum_{n=0}^{N-1} s_{m,n} g\left[k - m\frac{N}{2}\right] e^{j2\pi v\frac{n}{N}} e^{j\varphi_{m,n}} \cos\left(\frac{\pi k(2v+1)}{2V}\right), \quad 0 \le k \le K-1 \qquad (28)$$

Additionally, the modified GFDM signal as well as the elimination of its null coefficients are displayed in Equations (29) with (36) respectively:

$$R_{GFDM}[k] = (-1)^k \sum_{v=0}^{V-1}\sum_{b=0}^{B-1}\sum_{l=0}^{L-1}\sum_{n=0}^{N-1} s_n^b \left[\frac{B}{\lambda}\right] e^{j2\pi v\frac{(n-l)}{N}} \Big/ \sqrt{V} + \sqrt{\frac{2}{V}} \sum_{v=0}^{V-1}\sum_{b=0}^{B-1}\sum_{l=0}^{L-1}\sum_{n=0}^{N-1} s_n^b g[l] e^{j2\pi v\frac{(n-l)}{N}} \cos\left(\frac{\pi k(2v+1)}{2V}\right), \quad 0 \le k \le K-1 \qquad (29)$$

Equation (30) highlights the altered NOMA signal, while Equation (37) illustrates the removal of its null coefficients into account:

$$R_{NOMA}[k] = (-1)^k \sum_{v=0}^{V-1}\sum_{b=0}^{B-1}\sum_{m=0}^{M-1}\sum_{l=0}^{L-1}\sum_{n=0}^{N-1} \frac{s_{m,n}^{b} g_b[l] e^{j2\pi v\frac{(n-l-mc)}{N}}}{\sqrt{V}} + \sqrt{\frac{2}{V}} \sum_{v=0}^{V-1}\sum_{b=0}^{B-1}\sum_{m=0}^{M-1}\sum_{l=0}^{L-1}\sum_{n=0}^{N-1} s_{m,n}^{b} g_b[l] e^{j2\pi v\frac{(n-l-mC)}{N}} \cos\left(\frac{\pi k(2v+1)}{2V}\right), 0 \le k \le K-1 \qquad (30)$$

After applying a cosine filter, Y'[k] was divided into n seg portions, each with a length l seg, calculated using the Welsh segmentation method. Subsequently, the PSD of each segment was determined using the Hann window technique. The average of the previous PSDs was then used to derive the RPSD. RPSD serves as the basis for the decision statistic. As shown in Fig. 1, the segment is represented by the symbol "seg", and a windowed segment is referred to as "winseg".

After applying it on each grouping, the Hann window is multiplied by each one to obtain PSD. Where it is stated as:

$$PSD^{(j)}[k] = \frac{1}{L_{seg}} \left| \sum_{i=0}^{L_{seg}} R'^{[i]} Ham[i] \right|^2, \quad 0 \le k \le K-1, j = 1,2,\dots,N_{seg} \qquad (31)$$

$$R'_{F-MIMO-OFDM}[k] = R_{MIMO-F-OFDM}[k], \quad 0 \le k \le K'-1 \qquad (32)$$

$$R'_{MIMO-UFMC}[k] = R_{MIMO-UFMC}[k], \quad 0 \le k \le K'-1 \qquad (33)$$

$$R'_{MIMO-FBMC}[k] = R_{MIMO-FBMC}[k], \quad 0 \le k \le K'-1 \qquad (34)$$

$$R'_{MIMO-GFDM}[k] = R_{MIMO-GFDM}[k], \quad 0 \le k \le K'-1 \qquad (35)$$

$$R'_{MIMO-NOMA}[k] = R_{MIMO-NOMA}[k], \quad 0 \le k \le K'-1 \qquad (36)$$

R' stands for R'GFDM, R'UFMC, R'F-OFDM, R'FBMC, or R'NOMA in this instance. The following criteria are used to evaluate the mean PSDs:

$$RPSD = \frac{1}{N_{seg}} \sum_{i=0}^{N_{seg}-1} PSD(i) = G \qquad (37)$$

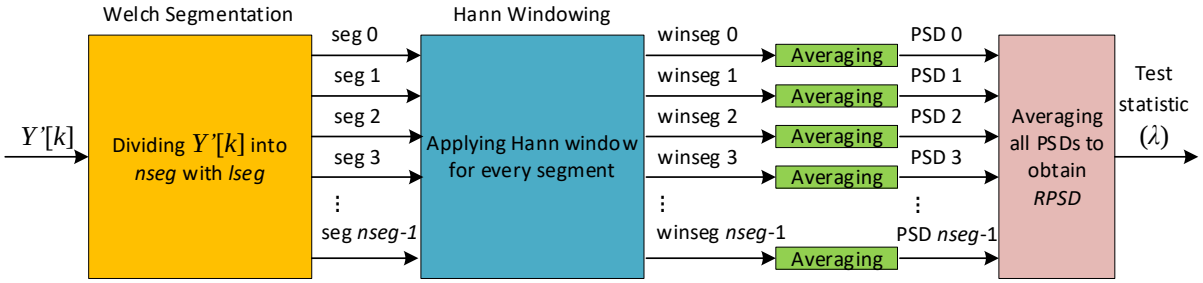

Fig. 1. The hybrid method in multi-kind of 5G waveforms.

Therefore, the binary hypothesis establishes H0, which refers to the possibility that λ is not greater or equal to λD, indicating that the 5G-MIMO (PU) signal that was received is entirely noise. The binary hypothesis also establishes if G is above λD, indicating that noise as well as one of its candidates are present in the received 5G-MIMO (PU) signal. This can be stated as:

$$\begin{cases} H_0, & G \leq> \lambda D \\ H_1, & G >> \lambda D \end{cases} \tag{38}$$

In Figure 2, each block receives a type of 5G waveform. The signals are then transformed from parallel fusion to serial fusion using the combiner. Next, the power of the resulting signal will be obtained from the two blocks separately to find the noise power and the traffic signal power. Finally, the noise power will be compared with the traffic signal power, and the test statistic will be obtained from the last block.

Additionally, since P_f depends on both the signal-to-noise ratio (SNR) and the initial length of the signal, it is determined using equation (13). However, the P_{fa} is computed in the following manner with the new length K':

$$P_{fa} = Q\left(\frac{\eta - \vartheta\left(\frac{\sigma_s^2}{\sigma_w^2}+1\right)}{\sqrt{\left(\frac{2}{K'}\right)\vartheta\left(\frac{\sigma_s^2}{\sigma_w^2}+1\right)}}\right) \tag{39}$$

V. Simulation Results

Throughout this section, modeling results—produced using MathWorks®—that assess the efficacy of five 5G waveforms—UFMC, GFDM, F-OFDM, NOMA, and FBMC—are showcased. The evaluation used AWGN channels with signal-specific characteristics and varied SNR levels. Table I in [26, 27] provides specific results for the UFMC, GFDM, F-OFDM, NOMA, and FBMC waveforms. It shows the results of simulations employing MathWorks® software, using the five 5G waveform choices: F-OFDM, UFMC, FBMC, GFDM, and NOMA. The system's performance is assessed at different levels of Signal-to-Noise Ratio (SNR) and in Additive White Gaussian Noise (AWGN) channels. The table provides results corresponding to different parameters associated with the generated GFDM, FBMC, UFMC, F-OFDM, and NOMA signals [32].

In Figure 3, the error likelihoods for -10 dB, -20 dB, and -35 dB SNR values were 0.051, 0.078, and 0.082, respectively, resulting in a false alarm rate of 0.05. As a result, at larger SNR values, the error likelihoods exhibited lower rates. At a -10 dB SNR value, the recommended (SS) method demonstrated a favorable error rate likelihood of 0.101. The traditional method, on the other hand, exhibited a higher error likelihood.

In Figure 4, the error likelihoods for -10 dB, -20 dB, and -35 dB SNR values were 0.058, 0.064, and 0.076, respectively, resulting in a false alarm rate of 0.05. As a result, at larger SNR values, the error likelihoods exhibited lower rates. At a -35 dB

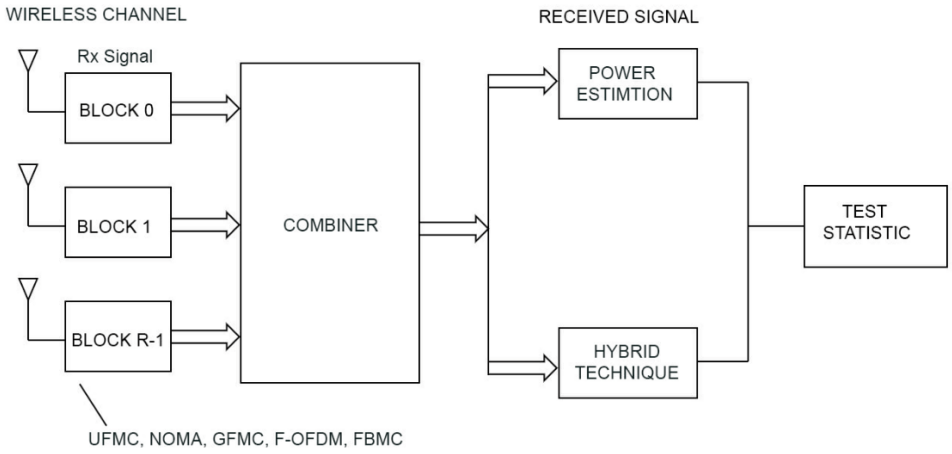

Fig. 2. Block diagram of the proposal system.

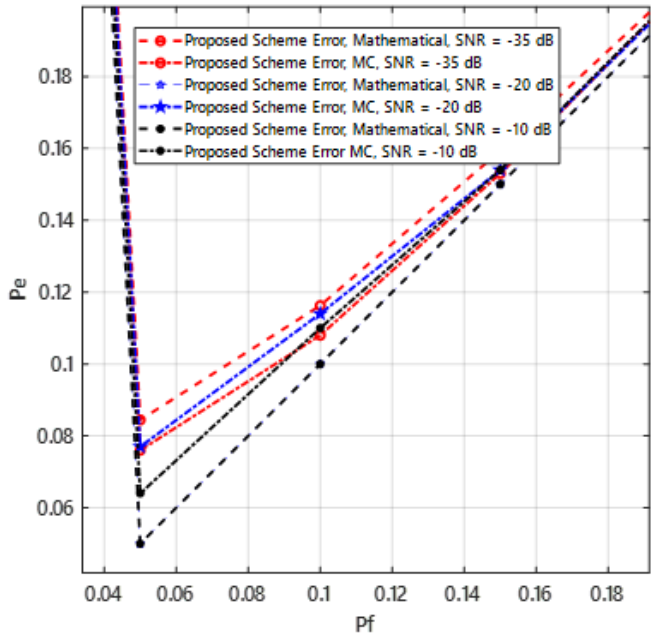

Fig. 3. Probability of error with probability of false alarm for FBMC.

SNR value, the recommended (SS) method demonstrated a favorable error rate likelihood of 0.076. The traditional method, on the other hand, exhibited a higher error likelihood. In Figure 5, the error likelihood for SNR values of -10 dB, -20 dB, and -35 dB were 0.05, 0.085, and 0.094, respectively, resulting in a false alarm rate of 0.05. As a result, at larger SNR values, the error likelihood exhibited lower rates.

At a -10 dB SNR value, the recommended (SS) method demonstrated a favorable error rate likelihood of 0.051. The traditional method, on the other hand, exhibited a higher error likelihood. In a similar manner, the best error likelihood for NOMA and GDFM is 0.05 at -10 dB, as shown in Figures 6 and 7, respectively. The parameters for the given SNR values indicate that the recommended (SS) technique performed better and identified the signal with lower error rates. The error probabilities associated with F-OFDM waveform identification are shown in Figure 4. A signal-to-noise ratio (SNR) of less than 0 dB was indicative of inadequate detection capabilities for the conventional mechanism. On the other hand, the suggested (SS) system demonstrated error probabilities that were consistently less than 1% across a range of SNR values, as demonstrated through both simulation and analytical calculations. As a result, the suggested (SS) architecture showed good signal recognition with a minimal chance of errors.

TABLE I
THE PARAMETERS OF DIFFERENT 5G WAVEFORM

GFDM	FBMC	UFMC	F-OFDM	NOMA
Number of FFT = 512	Number of FFT = 1024	Number of FFT = 512	Number of FFT = 1024	Number of FFT = 1024
Size of Sub-band = 20	Number of Guard = 212	Size of Sub-band = 20	Number of Resource Block = 50	Number of Resource Block = 50
Sub-bands number = 10	Symbols Overlapping = 4	Sub-bands number = 10	sub-carriers Number = 12	sub-carriers Number = 12
Length of cyclic prefix = 39	Number of Symbols = 100	Length of cyclic prefix = 43	Length of cyclic prefix = 72	Length of cyclic prefix = 88
Bits / Sub-carrier = 4	Bits / Sub-carrier = 2	Bits / Sub-carrier = 4	Bits / Sub-carrier = 6	Bits / Sub-carrier = 4
Offset of sub-band = 156		Offset of sub-band = 156	Offset tone = 2.5	Offset tone = 2.5
Filter length = 43		Filter length = 43	Filter length = 513	Filter length = 513

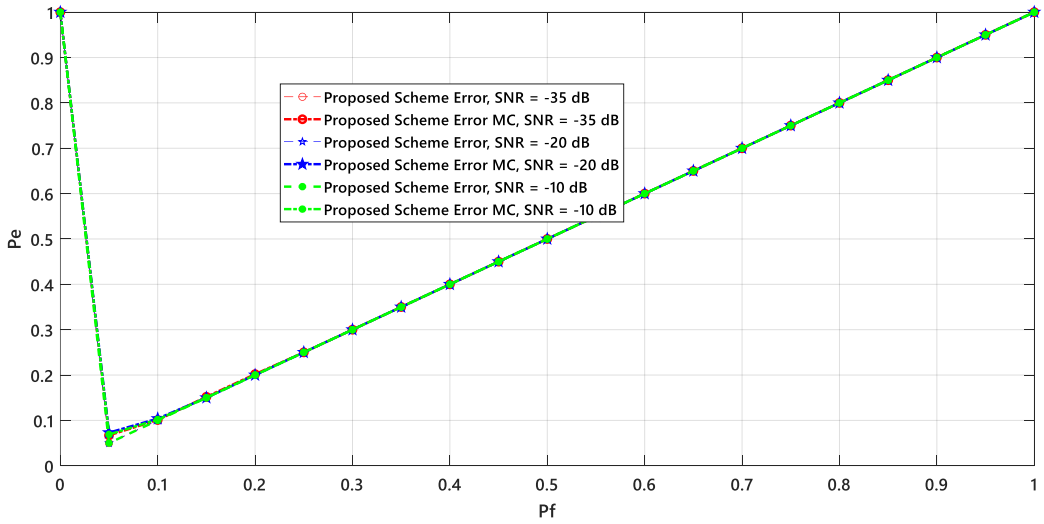

Fig. 4. Probability of error with probability of false alarm for F-OFDM.

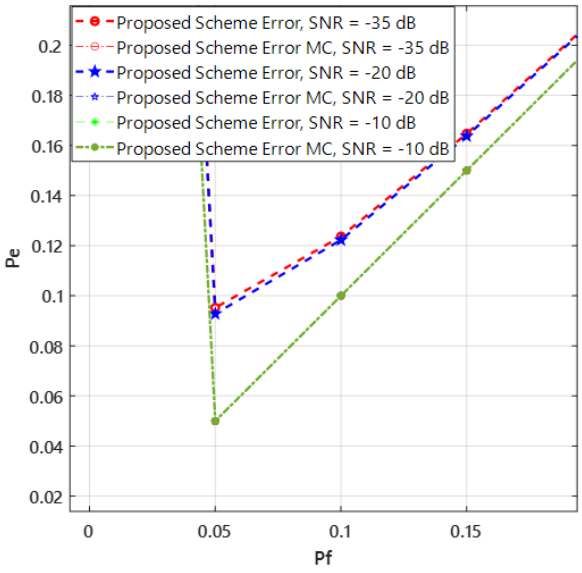

Fig. 5. Probability of error with probability of false alarm for UFMC.

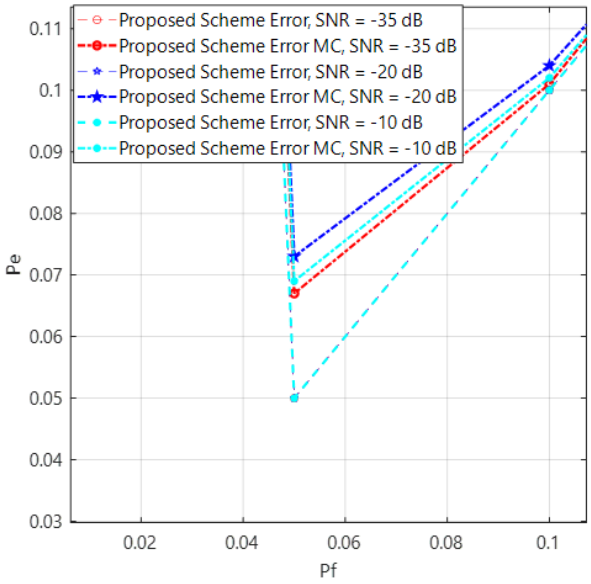

Fig. 7. Probability of error with probability of false alarm for GFDM.

After applying a 0.05 false alarm probability, the error and identification likelihoods were computed according to the mathematical model, resulting in (0.958, 0.092), (0.969, 0.081), and (0.985, 0.065) for SNR values of -35 dB, -20 dB, and -10 dB, respectively. The error likelihoods were found to be (0.072, 0.064, 0.059) for SNR values of -35 dB, -20 dB, and -10 dB, respectively, considering a false alarm likelihood of 0.05, as shown in Figure 3. The mathematical model was used in Figure 5 to determine the error likelihood as well as the signal recognition values. The results showed that the false alarm color. The error likelihoods for -35, -20, and -10dB SNR values were 0.069, 0.062, and 0.061, respectively, when a false alarm likelihood of 0.05 was considered. Consequently, the error probability was low for high SNR readings. At -35 dB SNR, the suggested (SS) method demonstrated a respectable error rate probability of 0.069. By comparison, as shown in Table II, the different values of Pe for five types of 5G waveforms indicated likelihood was 0.05 and the SNR values were -35 dB, -20 dB, and -10 dB, respectively: (0.958, 0.092), (0.969, 0.081), and (0.985, 0.065).

The error likelihood associated with the suggested (SS) technique is shown in Figure 6. Using Equation ($P_e = P_d + P_{md}$), all error probabilities pertaining to the simulation and mathematical frameworks were calculated. The colors green, blue, and red represent the parameters at SNR values of -10, -20, and -35 dB, respectively. For the two approaches, a similar error likelihood rate is indicated by two curves of the same that the error likelihood associated with the measured SNR values was comparatively higher with the traditional technique. The proposed (SS) framework showed a decrease in errors, enhancing the reliability of signal detection.

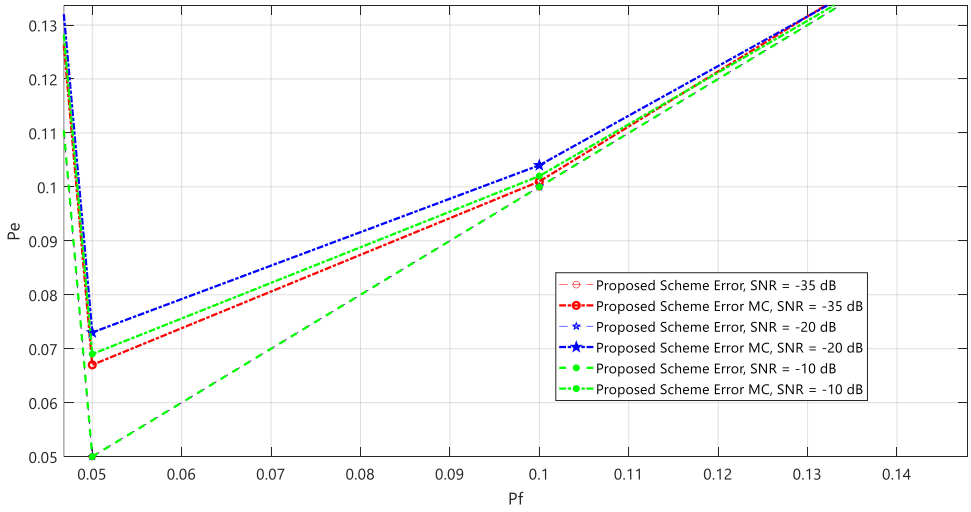

Fig. 6. Probability of error with probability of false alarm for NOMA.

TABLE II
THE DIFFERENT VALUE OF PE FOR 5 KINDS OF 5G WAVEFORMS

Figure of Merit	GFDM	FBMC	UFMC	F-OFDM	NOMA
Probability of error (-10)	0.66	0.5	0.89	0.6	0.43
Probability of error (-20)	0.73	0.5	098	0.79	0.55
Probability of error (-35)	0.72	0.5	0.99	0.8	0.54

VI. CONCLUSIONS

The paper investigated whether employing (HT) could reduce error rates and enhance detection performance in various SNR settings. To determine whether a signal is present or absent, our study compared averaged Power Spectral Densities (PSDs), which act as the test statistic, with predetermined thresholds. We evaluated the Receiver Operating Characteristic (ROC) curves for the proposed (SS) system and confirmed the accuracy of the mathematical (SS) theory using Monte Carlo experiments. Interestingly, the suggested (SS) system performed better even without requiring coherence with Primary Users (PUs) or pre-defined information quantities. It outperformed other methods in terms of detection likelihood, SNR threshold, and detection system error for all 5G waveforms, demonstrating its capacity to distinguish between traffic and noise. An obvious benefit was that the hybrid technique could be applied to all 5G waveform technologies.

Considering a false alarm likelihood of less than 0.05, a (Pd) of greater than 0.95, and a system error likelihood of less than 0.09%, the SS system achieved these results. For conventional 5G applications, this makes NOMA, GFDM, UFMC, F-OFDM, and FBMC feasible choices. Future study ideas include developing an outstanding performance both for cooperative and non-cooperative (SS) techniques that rely on hybrid filter detection. It is also recommended to investigate other performance measures and evaluate the suggested system in real-world cognitive radio scenarios to improve its capacity to detect signals missing in spectrum sharing.

REFERENCES

[1] X. Du et al. “Three-Dimensional Completion Method with Uniformity Decision Mechanism for Spectrum Sensing Data.” 2021 IEEE 21st International Conference on Communication Technology (ICCT), 13 Oct. 2021, https://doi.org/10.1109/icct52962.2021.9657954.

[2] W. Algriree, N. Sulaiman, M. M. Isa, R. K. Sahbudin, S. L. Hassan, and E. H. Salman, "On the Performance of Various 5G Signals Sensing Based on Hybrid Filter," International Journal of Wireless Information Networks, vol. 30, no. 1, pp. 42-57, 2023.

[3] T. Perarasi, G. Nagarajan, R. Gayathri, and M. Leeban Moses, "Evaluation of cooperative spectrum sensing with filtered bank multi carrier utilized for detecting in cognitive radio network," Transactions on Emerging Telecommunications Technologies, vol. 33, no. 7, p. e4478, 2022.

[4] H. S. Fouda, M. E. Nasr, and A. H. Hussein, "A highly efficient approach for performance enhancement of multiple antenna elements based spectrum sensing techniques using side lobe level reduction," Alexandria Engineering Journal, vol. 61, no. 8, pp. 5983-5999, 2022.

[5] D. A. Sehrai et al., "Metasurface-based wideband MIMO antenna for 5G millimeter-wave systems," IEEE Access, vol. 9, pp. 125348-125357, 2021.

[6] M. T. S. Hariom, H. P. Rana, and S. Nain, "Analysis of Spectrum Sensing Cognitive Radio Networks," 2022.

[7] W. Algriree et al., "An analysis of low complexity of 5G-MIMO communication system based CR using hybrid filter detection," Alexandria Engineering Journal, vol. 65, pp. 627-648, 2023.

[8] L. Bing, Li et al. “MIMO-NOMA Aided Healthcare IoT Networking: Automated Massive Connectivity Protocol.” IEEE Transactions on Consumer Electronics, vol. 69, no. 4, 1 Nov. 2023, pp. 697–708, https://doi.org/10.1109/tce.2023.3340322.

[9] W. Algriree, N. Sulaiman, M. Isa, R. K. Sahbudin, S. L. Hassan, and E. H. Salman, "Validation hybrid filter detection for Multi-User multiple input multiple output F-OFDM by Universal software radio Peripheral," Alexandria Engineering Journal, vol. 74, pp. 241-268, 2023.

[10] W. Algriree, N. Sulaiman, M. Isa, R. K. Z. Sahbudin, S. L. M. Hassan, and E. H. Salman, "The impact of M-ary rates on various quadrature amplitude modulation detection," International Journal of Electrical and Computer Engineering (IJECE), vol. 13, no. 1, pp. 483-492, 2023.

[11] M. M. Ali, and Mokhalad Khaleel Alghrairi, "Minimizing of Error Detection Using Bartlett-DCT Periodogram in Cognitive Radio Networks," J. Commun. , vol. 14, no. no. 5, pp. 363-367, 2019.

[12] M. Ali and H. Nam, "Effect of spectrum sensing and transmission duration on spectrum hole utilisation in cognitive radio networks," IET Communications, vol. 11, no. 16, pp. 2539-2543, 2017.

[13] D. K. Patel, B. Soni, and M. López-Benítez, "Improved likelihood ratio statistic-based cooperative spectrum sensing for cognitive radio," IET Communications, vol. 14, no. 11, pp. 1675-1686, 2020.

[14] X. Liu and K. Zheng, "Probability-based fusion rule in cooperative spectrum sensing with impact of geographic location," IET Communications, vol. 16, no. 9, pp. 963-976, 2022.

[15] K. K. Godugu and S. Vappangi, "Performance evaluation of hard-decision and soft-data aided cooperative spectrum sensing over Nakagami-m fading channel," IET Communications, vol. 17, no. 13, pp. 1492-1512, 2023.

[16] Z. Shi, Y. Zhang, Z. Qian, X. Sun, and X. Ma, "Compressive narrowband interference detection and parameter estimation in direct sequence spread spectrum communication," IET Signal Processing, vol. 16, no. 1, pp. 14-25, 2022.

[17] H. Al-amaireh and Z. Kollar, "Reducing the complexity of FS-FBMC receivers using hopping DFT," in 2019 29th International Conference Radioelektronika (RADIOELEKTRONIKA), 2019: IEEE, pp. 1-5.

[18] H. Kim, Y. Park, J. Kim, and D. Hong, "A low-complex svd-based f-ofdm," IEEE Transactions on Wireless Communications, vol. 19, no. 2, pp. 1373-1385, 2019.

[19] H. Wang, L. Xu, Z. Yan, and T. A. Gulliver, "Low-complexity MIMO-FBMC sparse channel parameter estimation for industrial big data communications," IEEE Transactions on Industrial Informatics, vol. 17, no. 5, pp. 3422-3430, 2020.

[20] S. Salar Hosseini, M. R. Javan, and A. Nazari, "Multicasting in NOMA-based UAV networks: Path design and throughput maximisation," IET Communications, vol. 16, no. 14, pp. 1708-1723, 2022.

[21] Z. Guo, Q. Liu, W. Zhang, and S. Wang, "Low complexity implementation of universal filtered multi-carrier transmitter," IEEE Access, vol. 8, pp. 24799-24807, 2020.

[22] S. A. Fathy, M. Ibrahim, S. El-Agooz, and H. El-Hennawy, "Low-complexity SLM PAPR reduction approach for UFMC systems," IEEE Access, vol. 8, pp. 68021-68029, 2020.

[23] I. Baig, U. Farooq, N. U. Hasan, M. Zghaibeh, and V. Jeoti, "A multi-carrier waveform design for 5G and beyond communication systems," Mathematics, vol. 8, no. 9, p. 1466, 2020.

[24] X. Liu, Q. Sun, W. Lu, C. Wu, and H. Ding, "Big-data-based intelligent spectrum sensing for heterogeneous spectrum communications in 5G," IEEE Wireless Communications, vol. 27, no. 5, pp. 67-73, 2020.

[25] R. Gerzaguet et al., "The 5G candidate waveform race: a comparison of complexity and performance," EURASIP Journal on Wireless Communications and Networking, vol. 2017, pp. 1-14, 2017.

[26] S. R. Ahmed, A. S. Abdullah, and N. M. Hammash, "Universal filtered multicarrier (UFMC) vs. orthogonal frequency division multiplexing (OFDM)," in Journal of Physics: Conference Series, 2020, vol. 1530, no. 1: IOP Publishing, p. 012092.

[27] E. A. Armas Vega, A. L. Sandoval Orozco, L. J. Garcia Villalba, and J. Hernandez-Castro, "Digital images authentication technique based on dwt, dct and local binary patterns," Sensors, vol. 18, no. 10, p. 3372, 2018.

[28] Z. Hua, Y. Zhou, and H. Huang, "Cosine-transform-based chaotic system for image encryption," Information Sciences, vol. 480, pp. 403-419, 2019.

[29] J. Abdoli, M. Jia, and J. Ma, "Filtered OFDM: A new waveform for future wireless systems," in 2015 IEEE 16th international workshop on signal processing advances in wireless communications (SPAWC), 2015: IEEE, pp. 66-70.

[30] M. Schellmann et al., "FBMC-based air interface for 5G mobile: Challenges and proposed solutions," in 2014 9Th international conference on cognitive radio oriented wireless networks and communications (CROWNCOM), 2014: IEEE, pp. 102-107.
[31] T. Wild, F. Schaich, and Y. Chen, "5G air interface design based on universal filtered (UF-) OFDM," in 2014 19th International Conference on Digital Signal Processing, 2014: IEEE, pp. 699-704.
[32] Z. T. Yaseen and W. Algriree, "Reliable 5G waveform detection from an optical fibre transmitter system," Opto-Electronics Review, pp. e149181-e149181, 2024.

Mokhalad Alghrairi is a Lecturer at the Department of Computer Techniques Engineering, Imam Al Kadhim College (IKC). He Received a B.Sc degree in 2006 from Al-Mustansiriya University, Iraq, and M.Sc. degree in 2016 from University Putra Malaysia (UPM). He also obtained a Ph.D. degree in Electronic Engineering from University Putra Malaysia (UPM), Malaysia in 2023. The field of interest, cognitive radio, Microelectronics, MIMO, Designing implantable micro-system stimulators, bio-medical implantable devices, healthcare monitoring and inductive coupling links for biomedical applications. mokhalad.khaleel@iku.edu.iq.

Aqeel kamil Kadhim has done PhD in Computer Engineering and currently works as a faculty member in the Department of Computer Technology Engineering at Imam Al-Kadhim College - Baghdad. He teaches undergraduate students and has a large number of international and national publications, and has written a book on information technology. His research interests include sensor network applications, image processing, information technology in management, and performance evaluation of information systems that include wireless systems and application software. He is a member of IEEE and ACM. compeng.lecturer4@alkadhum-col.edu.iq.

Manar Adnan Nassrat is a Lecturer at the Department of Optics Technique, Al-Hikma University College. She received his B.Sc. in Communication Engineering. Her research interests include image processing, information technology in management, and performance evaluation of information systems that include wireless systems and application software.

Bayan Mahdi Sabbar received his B.Sc. in Electrical Engineering, in 1980, M.Sc. in Digital Communications Systems, in 1983, and Ph.D in (Electrical Engineering)/ high resolution array Signal Processing, in 1987. Currently, he is a head of Control Engineerin Department, AlNahrain University, Baghdad, Iraq. His Fields of Interest are Adaptive systems, High resolution algorithms and their applications, Applications of Signal Processing in Direction Finding and Image Processing, and Identifications Systems based on Signal Processing.

Saad Mutashar was born in Baghdad, Iraq 1961. Received B.Sc and M.Sc degrees in 1984 and 1986 respectively from University of Belgrade, Serbia. In 2014, he received his PhD degree from National University of Malaysia (UKM). Since 2005 he is an assist professor at the Department of Electrical Engineering, University of Technology, Iraq. The field of interest, Microelectronics, Designing implantable micro-system stimulator, bio-medical implantable devices and inductive coupling links for bio-medical applications. More than 40 published papers at international scientific journals. Editor board and reviewer in several journals. He is an IEEE member. Saad.Mutashar.abbas@uomus.edu.iq. ORCID=0000-0002-3510-9423.